

Dedicated
to
My Beloved Parents

MOSARRAF HOSSAIN

SIULI BIBI

DECLARATION

I, **Sahin Reja**, hereby declare, that the work presented in this thesis entitled “Polydentate ligand based metal complexes for oxidase activity” is an authentic record of research work done by me under the supervision of Dr. Rajesh Kumar Das, Assistant Professor, Department of Chemistry, University of North Bengal, Darjeeling, West Bengal, India

The research work in this thesis (in full) has not been submitted elsewhere earlier, for the award of any other degree, diploma and fellowship to this or any other University/Institute.

Sahin Reja

Sahin Reja

Department of Chemistry
University of North Bengal

Date: 07.11.2023

UNIVERSITY OF NORTH BENGAL

RAJESH DAS, Ph.D
Assistant Professor
Department Of Chemistry
University of North Bengal
Darjeeling, 734013

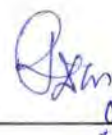


Cell: +91 9434459238
Email: rajeshnbu@gmail.com
rajeshkumardas@nbu.ac.in

ENLIGHTENMENT TO PERFECTION
Accredited by NAAC with grade B++

CERTIFICATE

This is to certify that the thesis entitled "**Polydentate ligand based metal complexes for oxidase activity**" is an authentic record of research work carried out by **Mr. Sahin Reja** for fulfilment of the requirements for the degree of "DOCTOR OF PHILOSOPHY IN CHEMISTRY" under my supervision at University of North Bengal, Darjeeling, West Bengal, India. I further certify that this research work is original, and no part of this thesis has been submitted for the award of any degree or diploma to this or any other University/Institute.


02/11/2023

Dr. Rajesh Kumar Das
Department of Chemistry
University of North Bengal

Dr. Rajesh Kumar Das
Assistant Professor
Department of Chemistry
University of North Bengal
Darjeeling - 734013, India

Anti-Plagiarism Report of the Ph.D Thesis

Title of the Thesis:


Polydentate ligand based metal complexes for oxidase activity

Original
by Turnitin

Document Information

Analyzed document	Sahin Reja_Chemistry.pdf (D174868369)
Submitted	9/29/2023 11:42:00 AM
Submitted by	University of North Bengal
Submitter email	nbuplg@nbu.ac.in
Similarity	0%
Analysis address	nbuplg.nbu@analysis.arkund.com

Sahin Reja 07.11.2023
Signature of the Candidate


07-11-2023
Signature of the Supervisor

Dr. Rajesh Kumar Das
Assistant Professor
Department of Chemistry
University of North Bengal
Darjeeling - 734013, India

PREFACE

I started the research work presented in this thesis entitled “Polydentate ligand based metal complex for oxidase activity” in the year 2019 under the supervision of Dr. Rajesh Kumar Das in the Department of Chemistry, University of North Bengal, India. In recent years, the study of metal complexes with polydentate ligands has gained significant attention due to their potential applications in various fields, such as catalysis, biological activity, and materials science. Among them, metal complexes with polydentate ligands have been found to exhibit remarkable oxidase activity, making them a promising candidate for developing efficient and selective oxidase mimics.

*The thesis starts with **Chapter I** where a detailed study of different types of ligands, metal complexes, oxidase activity and biological activity are described. **Chapter II** discusses all the methodologies associated with synthesis of ligand and metal complexes techniques in detail. A novel compound, 3-(1,3-dioxisoindolin-2-yl)-N,N-dimethyl propan-1-aminium perchlorate (DIDAP), was successfully synthesized and characterized through various spectroscopic techniques, including single crystal X-ray diffraction, as discussed in **Chapter III**. DIDAP was found to self-assemble into a helical structure with strong intermolecular interactions in its solid state and exhibited promising anticancer activity against the Hep G2 cell line, supported by docking studies and computational analysis of its chemical reactivity. **Chapter IV** encompasses a novel compound, 3,3'-[succinylbis(diazaneyl)]bis(N,N,N-trimethylpropan-1-ammonium) perchlorate (SAPAP), synthesized from N1, N4- Bis(3-(dimethylamino)propyl)succinamide (DAPS), which demonstrated exceptional anticancer activity against human colon carcinoma cells (HT-29), highlighting its potential as a promising candidate for future anticancer therapies, supported by comprehensive evaluations including docking, molecular dynamics simulations, pharmacokinetic predictions, and ELISA assays. **Chapter V** describes a newly synthesized copper-based complex $[Cu_2L_2(OAc)_4]$ with 2-(3-(dimethylamino)propyl)isoindoline-1,3-dione as a ligand that exhibits dual enzymatic activities, acting as a catechol oxidase and phenoxazinone synthase under aerobic conditions, supported by various analyses, while also demonstrating significant anti-leukemic and anti-bacterial properties, making it a versatile bioinspired metallocatalyst with potential therapeutic applications. In **Chapter VI**, a novel copper-based metallocatalyst $[Cu(L1)_2(L2)]$ featuring P-hydroxybenzoic acid and N1,N1-dimethylpropane-1,3-*

*diamine ligands that exhibits unique catechol oxidase and phenoxazinone synthase activities, characterized by distorted geometry, intricate molecular interactions, and oxygen-dependent enzymatic radical pathways, with exceptionally high catalytic efficiency and the generation of hydrogen peroxide as a key mechanistic feature. **Chapter VII** includes future research in polydentate ligand-based metal complexes aiming to enhance oxidase activity that has the potential to yield novel multifunctional complexes with diverse applications in biotechnology, medicine, energy conversion, and industry, driving innovation across multiple disciplines.*

ACKNOWLEDGEMENTS

It will be very difficult for me to mention each and every one and their contribution in this research work, but I want to take this opportunity to express my appreciation to a few who played a key role.

At first, on top for all, I owe many thanks to the almighty Allah for his protection and guidance in all aspects of my life.

*Next, I would like to express my sincere thanks and gratitude to my research supervisor **Dr. Rajesh Kumar Das** for his able guidance, valuable ideas, comments, expert teaching skill, valuable time, and tireless effort in supporting and supervising me. I would like to convey my sincere gratitude to **Prof. Somobrata Acharya**, School of Applied & Interdisciplinary Sciences, Indian Association for the Cultivation of Science, Jadavpur, for XRD facility.*

I am very much obliged to University of North Bengal for giving me the opportunity to pursue Ph. D. and all Staffs of the University of North Bengal for various official supports during the research work.

I would also like to express my gratefulness to the Department of Chemistry, University of North Bengal for providing me with all the support and facilities for my research work. I am extremely grateful to all the faculty members of the Department of Chemistry for their constant support and valuable suggestion during my work. I am also thankful to all the technical staff, laboratory assistants and non-teaching staff for their kind support during the research work.

I wish to express my warm and sincere thanks to my lab mates Deboshmita Mukherjee, Kaushik Sarkar, Md. Bakibillah, Dilip Sarkar and Sumana Roy for their assistance. My sincere thank goes to the research scholar, Subhajit Sarkar for his valuable suggestions and continuous cooperation throughout my research work.

Last but not the least, my sincere thanks, deepest gratitude and hearty love to my mother Siuli Bibi, father Mosarraaf Hossain and younger brother Md Soyel Rana, and friend Tahera Naj for their unending love and support.

Sahin Reja

LIST OF TABLES

Chapter	Table No.	Title of the Table	Page No.
Chapter II	2.1	Purity and source of the chemicals used.	33
Chapter III	3.1	Hydrogen bonded geometries in DIDAP .	73
	S3.1	Analytical and physical data of the synthesized ligand and compound.	89
	S3.2	Crystal data collection and structure refinement for DIDAP .	89
	S3.3	Selected bond lengths (Å), bond angles (°) and torsion angles (°) for DIDAP .	91
Chapter IV	4.1	Quantum Chemical Descriptors for the SAPAP the B3LYP/6-31G Level of Theory.	98
	4.2	Crystal data collection and structure refinement for SAPAP.	101
	4.3	Hydrogen bonded geometries in SAPAP.	102
	S4.1	Predicted Drug-Likeness and Pharmacokinetic Properties of SAPAP	122
	S4.2	Selected bond lengths (Å), bond angles (°) and torsion angles (°) for SAPAP	122
Chapter V	5.1	Crystal data collection and structure refinement for complex.	128
	S5.1	Kinetic parameters for the oxidation of 3,5-DTBC catalyzed by complex.	171
	S5.2	Kinetic parameters for the oxidation of 2-AP catalyzed by complex.	171
	S5.3	Quantum Chemical Descriptors of the binuclear Cu-complex.	172
	S5.4	Selected bond lengths (Å), bond angles (°) and torsion angles (°) for Complex.	172
	S5.5	Hydrogen bonded geometries in Complex.	173
	S5.6	X-H...Cg(Pi-Ring) Interactions.	173
Chapter VI	6.1	Crystal data collection and structure refinement for complex.	178
	S6.1	Selected bond lengths (Å), bond angles (°) and torsion angles (°) for Complex.	212
	S6.2	Hydrogen bonded geometries in Complex.	212
	S6.3	X-H...Cg(Pi-Ring) Interactions for Complex.	213

S6.4	Kinetic parameters for the oxidation of 3,5-DTBC catalyzed by complex.	213
S6.5	Kinetic parameters for the oxidation of 2-AP catalyzed by complex.	213

LIST OF FIGURES

Chapter	Figure No.	Title of the Figure	Page No.
Chapter I	1.1	A library of ligands.	2
	1.2	A library of monodentate ligands.	4
	1.3	A library of bidentate ligands.	5
	1.4	A library of polydentate ligands.	7
	1.5	Some metal complexes.	10
	1.6	Crystal field splitting.	12
	1.7	The conversion of 3,5-di-tert-butylcatechol (3,5-DTBC) to 3,5-di-tertbutyl benzoquinone (3,5-DTBQ).	17
	1.8	Catalytic cycle for catecholase activity as suggested from the literature	20
	1.9	Catalytic cycle for catecholase activity as proposed by Siegbahn based on DFT calculation.	21
	1.10	The conversion of o-Aminophenol (2-AP) to 2-Aminophenoxazine-3-one (APX).	22
Chapter II	2.1	Ambient temperature reaction setup.	36
	2.2	Reflux reaction setup.	38
	2.3	Slow evaporation process.	43
	2.4	Bilayer process.	44
	2.5	Diffusion process	45
	2.6	Jasco Fourier Transform Infrared Spectrometer	52
	2.7	Bruker Avance-II 400 MHz NMR Spetrometer	54
	2.8	The Bruker EMX EPR spectrometer	56
	2.9	Bruker single crystal XRD	58
Chapter III	3.1	Schematic representation of the work.	68
	3.2	The ORTEP diagram with ellipsoid of 40% probability.	73
	3.3	Intermolecular hydrogen bonding interactions in DIDAP .	74
	3.4	$Cg \cdots Cg$ interactions in DIDAP $Cg1$ and $Cg2$ are the centroids of N1–C8 and C1–C6 rings respectively. <i>Symmetry codes: (iv) $-1/2+x, 1/2-y, z$; (v) $1/2+x, 1/2-y, z$.</i>	74
	3.5	(a) Formation of helix like arrangement of cationic units in DIDAP along the c axis, two parallel strands have been shown with one strand in space fill model for better understanding; (b) Each screw-pitch contains one perchlorate ion in the helix like architecture of DIDAP .	75
	3.6	Hirshfeld surfaces mapped with d_{norm} (left-side), shape index (middle) and curvedness(right-side).	76

3.7	Fingerprint plot: Full (1st row left-side) and resolved into O···H/H···O, H···H, C···C, C···H / H···C contact contributed to the total Hirshfeld Surface area of compound.	78
3.8	Hep-G2 liver cancer cell growth inhibition curves for DIDAP compound.	79
3.9	Compound docked in liver cancer protein (PDB: 2JW2) with (a) 3D binding mode interaction into the binding pocket of receptor in two different style (adriamycin as green colour stick and amino acids as blue) and (b) 2D binding interaction of adriamycin with different amino acids of the receptor (hydrogen bond is shown as deep green dash line).	81
S3.1	¹ H-NMR Spectrum of DAPID.	86
S3.2	¹ H-NMR Spectrum of DIDAP.	86
S3.3	¹³ C-NMR Spectrum of DAPID.	87
S3.4	¹³ C-NMR Spectrum of DIDAP.	87
S3.5	FT-IR spectrum of DIDAP.	88
S3.6	UV-Visible spectra of DIDAP in acetonitrile solution.	88
S3.7	Mass spectrum of DIDAP.	89
S3.8	Molecular packing diagram of DIDAP in <i>ab</i> plane.	91
S3.9	(a) Image of the optimized structure of compound. (b) Image of HOMO-LUMO energy gap.	92
S3.10	Adriamycin docked in liver cancer protein (PDB: 2JW2) with (a) 3D binding mode interaction into the binding pocket of receptor (compound as green colour stick and amino acids as blue) and (b) 2D binding interaction of compound with different amino acids of the receptor (hydrogen bond is shown as deep green dash line)	93
<hr/>		
Chapter IV	4.1 Schematic representation of the work.	95
	4.2 The asymmetric unit of SAPAP, ORTEP diagram drawn with ellipsoid of 50% probability.	101
	4.3 The complete molecule of SAPAP, ORTEP diagram drawn with ellipsoid of 50% probability (perchlorate ions excluded for clarity).	101
	4.4 Intramolecular and intermolecular Hydrogen bonding interactions in SAPAP.	103
	4.5 Helical arrangement in SAPAP , dotted lines indicate hydrogen bonding interactions.	103
	4.6 Hirshfeld surfaces mapped with d_{norm} (left-side), shape index (middle) and curvedness (right-side).	105
	4.7 Fingerprint plot: Full (1st row left-side) and resolved into O···H/H···O, H···H, C···H / H···C, O----N/N----O, C----O/O--	106

		---C contact contributed to the total Hirshfeld Surface area of compound.	
4.8		Energy-framework diagrams for Edis for a cluster of molecule. The cylindrical radius is proportional to the relative strength of the corresponding energy and was adjusted to the scale factor of $-13.2 \text{ kJ mol}^{-1}$ with a cut-off value of 10 kJ mol^{-1} .	106
4.9		HT-29 colon carcinoma cancer cell growth inhibition curves for SAPAP compound along with blank control.	107
4.10		Molecular docking interaction of SAPAP with colon cancer target (PDB ID: 3IG7).	109
4.11		Root mean square deviation (RMSD), root mean square fluctuation (RMSF), radius of gyration (Rg), and SASA plots of protein-SAPAP complex.	110
4.12		Effect of SAPAP on IL-6 and COX-2 activity using HT-29 colon carcinoma cancer cells	111
S4.1		$^1\text{H-NMR}$ Spectrum of DAPS .	116
S4.2		$^1\text{H-NMR}$ Spectrum of SAPAP .	117
S4.3		$^{13}\text{C-NMR}$ Spectrum of DAPS .	118
S4.4		$^{13}\text{C-NMR}$ Spectrum of SAPAP .	119
S4.5		FT-IR spectrum of SAPAP .	120
S4.6		UV-Visible spectra of SAPAP in dimethyl sulfoxide solution.	120
S4.7		Packing diagram in SAPAP .	121
S4.8		Frontier molecular orbitals of SAPAP with their band gap energies	121
<hr/>			
Chapter V	5.1	Flowchart of the work.	124
	5.2	Asymmetric unit of complex, with displacement ellipsoids drawn at the 30% probability level.	129
	5.3	Intramolecular hydrogen bonding interactions in Complex in bc plane.	130
	5.4	X--H \cdots Cg interactions in complex, where Cg2, Cg3 are the centroids of C2-C7, N1-C8, rings respectively. <i>Symmetry code</i> : $1/2 - x, -1/2 + y, 1/2 - z$.	130
	5.5	Polyhedral view of complex.	131
	5.6	The Cyclic voltammogram of the (a) complex, (b) complex with 3,5 DTBC, (c) complex with 2-AP under molecular oxygen atmosphere in anhydrous methanol medium (0.20 M tetrabutylammonium perchlorate) at 295 K.	133
	5.7	Ground state optimised B1 and B2 geometries with matching potential energy values were obtained using the theoretical DFT/B3LYP/6-311G/LANL2DZ approach.	134
	5.8	X- band EPR spectra of complex and complex with 2-AP after 10 min in MeOH solution at 298 K.	136
	5.9	Ground state optimised B1 and B2 geometries with matching potential energy values were obtained using the theoretical	137

	DFT/B3LYP/6-311G/LANL2DZ approach.	
5.10	Disc Diffusion Assay of complex against <i>B. cereus</i> and <i>E.coli</i>	137
5.11	MIC Assay of complex against <i>B. cereus</i> and <i>E.coli</i> at varying concentrations.	138
5.12	(A) Normal hepatic HL-7702 cell growth inhibition curves for Complex (B)Hep-G2 liver cancer cell growth inhibition curves for Complex.	138
5.13	Molecular docking interaction of binuclear Cu-complex with liver cancer-2 (PDB ID: 2JW2) receptor.	140
S5.1	¹ H-NMR Spectrum of DAPD.	154
S5.2	¹³ C-NMR Spectrum of DAPD.	154
S5.3	FT-IR spectrum of DAPD.	155
S5.4	UV-Visible spectra of DAPD in methanol solution.	155
S5.5	UV-Visible spectra of complex in methanol solution.	156
S5.6	FT-IR spectrum of complex.	156
S5.7	Mass spectrum of complex	157
S5.8	Change in spectral pattern of complex after reaction with 3,5-DTBC, observing the reaction for 2h in methanol. This repetitive spectra were obtained in 5 min interval at room temperature. The peak for the coloured product (3,5-DTBQ) appears at 390 nm which gradually shifts to 401 nm.	158
S5.9	A plot of the difference in absorbance (ΔA) vs. time to evaluate the rate of catalysis of 3,5-DTBC by complex in methanol.	159
S5.10	Plot of rate vs. [substrate] (3,5-DTBC) in presence of complex in MeOH.	159
S5.11	Line weaver–Burk plot. of 3,5-DTBC	160
S5.12	Change in spectral pattern of complex in MeOH after reaction with 2-AP, monitoring the reaction for 2h.	160
S5.13	A plot of the difference in absorbance (ΔA) vs. time to evaluate the rate of catalysis of 2-AP by complex in methanol.	161
S5.14	Plot of rate vs. [substrate] (2-AP) in presence of complex in MeOH.	161
S5.15	Line weaver–Burk plot. of 2-AP.	162
S5.16	(a) Side view, and (b) top view of the DFT optimized structure of binuclear Cu-complex.	162
S5.17	Dimerized structure of complex.	163
S5.18	Packing diagram of complex along <i>b</i> axis.	163
S5.19	Hirshfeld surfaces mapped with d_{norm} (left-side), shape index (middle) and curvedness (right-side).	165
S5.20	Fingerprint plot: Full (1 st row left-side) and resolved into C···C, C···H / H···C, C···N/ N···C, H···H, N···H/H···N, C···O / O···C, O···H/H···O, O···O contact contributed to the total Hirshfeld Surface area of compound.	167

	S5.21	Mass spectrum of complex with 3,5-DTBC.	167
	S5.22	Plausible mechanistic pathways for the catalytic oxidative coupling of 3,5-DTBC by this dicopper(II) complex.	169
	S5.23	Plausible mechanistic pathways for the catalytic oxidative coupling of 2-AP by this dicopper(II) complex.	170
	S5.24	HOMO and LUMO of the DFT optimized structure of binuclear Cu-complex.	171
	S5.25	MEP surface of binuclear Cu-complex.	171
<hr/>			
Chapter VI	6.1	Flowchart of the work.	177
	6.2	Ortep view of the asymmetric unit with 30% probability.	180
	6.3	Intermolecular hydrogen bonding interactions in complex along <i>b</i> axis.	181
	6.4	Intramolecular hydrogen bonding interactions in complex along <i>b</i> axis.	181
	6.5	The spectral pattern of complex undergoes a significant alteration upon reaction with 3,5-DTBC, while monitoring the reaction in methanol for a duration of 2 hours. A series of spectra were acquired at 5-minute intervals at room temperature. A noticeable peak corresponding to the formation of the colored product (3,5-DTBQ) emerges at 390 nm, which subsequently shifts gradually to 401 nm.	184
	6.6	Plot of rate vs. [substrate] (3,5-DTBC) in presence of complex in MeOH.	184
	6.7	The cyclic voltammogram of the (a) complex, (b) complex with 3,5 DTBC, (c) complex with 2-AP under molecular oxygen atmosphere in anhydrous methanol medium (0.20 M tetrabutylammonium perchlorate) at 295 K.	185
	6.8	X- band EPR spectra of complex, complex with 3,5-DTBC and complex with 2-AP after 10 min in MeOH solution at 298 K.	186
	6.9	Ground state optimised B1 and B2 geometries with matching potential energy values were obtained using the theoretical DFT/B3LYP/6-311G/LANL2DZ approach.	186
	6.10	Change in spectral pattern of complex in MeOH after reaction with OAPH, observing the reaction for 2h.	189
	6.11	Plot of rate vs. [substrate] (2-AP) in presence of complex in MeOH.	189
	6.12	Ground state optimized geometries of B1 and B2 with corresponding potential energy values during the course of Cu complex with 2AP employing DFT/B3LYP/6-311G/LANL2DZ theoretical method	190
	S6.1	Hirshfeld surfaces mapped with d_{norm} (left-side), shape index (middle) and curvedness (right-side).	200
<hr/>			

S6.2	Fingerprint plot: Full (1 st row left-side) and resolved into H···H, O···H / H···O, C···H / H···C, C···C, C···O / O···C, O···O contact contributed to the total Hirshfeld Surface area of compound.	202
S6.3	C--H···C _g interactions in complex, where C _g 5 and C _g 10 are the centroids of C9–C14 ^{vi} , Cu2-O8 ^{iv} , Cu1-O11 ^{iv} and C28–C33 ^{vii} rings respectively. <i>Symmetry codes: (vi) -I+x, y, z; (vii) x, y, I+z.</i>	203
S6.4	Polyhedral view of complex.	203
S6.5	UV-Visible spectra of complex in methanol solution.	204
S6.6	A plot of the difference in absorbance (ΔA) vs. time to evaluate the rate of catalysis of 3,5-DTBC by complex in methanol.	204
S6.7	Plausible mechanistic pathways for the catalytic oxidative coupling of 3,5-DTBC by this dicopper(II) complex.	206
S6.8	A plot of the difference in absorbance (ΔA) vs. time to evaluate the rate of catalysis of 2-AP by complex in methanol.	207
S6.9	Plausible mechanistic pathways for the catalytic oxidative coupling of 2-AP by this dicopper(II) complex.	207
S6.10	FT-IR spectrum of complex.	208
S6.11	Line weaver–Burk plot. of 3,5-DTBC.	208
S6.12	Line weaver–Burk plot. of 2-AP.	209

LIST OF APPENDICES

Appendix	Title of the Topic	Page No.
I	List of Publications.	221
II	List of Communicated Articles.	223
III	List of Seminars, Webinars and Symposiums presented.	224